

Communication

Control of Spectral and Polarization Properties of Quasiunipolar Terahertz Pulses in Strongly Nonequilibrium Magnetized Plasma Channels

Anna V. Bogatskaya ^{1,2} , Ekaterina A. Volkova ³ and Alexander M. Popov ^{1,2,*} ¹ Department of Physics, Moscow State University, Moscow 119991, Russia; annabogatskaya@gmail.com² P.N. Lebedev Physical Institute, Russian Academy of Sciences, Moscow 119991, Russia³ D.V. Skobeltsyn Institute of Nuclear Physics, Moscow State University, Moscow 119991, Russia; evolkova@mics.msu.su

* Correspondence: alexander.m.popov@gmail.com

Abstract: The possibility to control both spectral and polarization properties of seed THz pulses in strongly nonequilibrium elongated magnetized plasma channels formed via intense UV femtosecond laser pulses in nitrogen (air) is analyzed. The physical mechanism of THz pulse control is based on cyclotron resonance, which can strongly reconstruct electrodynamic plasma features and, in particular, its ability to amplify the radiation of different spectral bands and polarization states. In particular, the formation of quasiunipolar pulses with a non-zero electric area and a specific polarization state is discussed. This study is based on the self-consistent solution of the kinetic Boltzmann equation for the electron velocity distribution function (EVDF) in the plasma channel and the second-order wave equation for THz pulse propagation.

Keywords: terahertz generation from plasma; electron velocity distribution function; magnetized plasma; cyclotron resonance; quasiunipolar pulses; nonequilibrium plasma; numerical modeling



Citation: Bogatskaya, A.V.; Volkova, E.A.; Popov, A.M. Control of Spectral and Polarization Properties of Quasiunipolar Terahertz Pulses in Strongly Nonequilibrium Magnetized Plasma Channels.

Photonics **2023**, *10*, 585. <https://doi.org/10.3390/photonics10050585>

Received: 12 April 2023

Revised: 2 May 2023

Accepted: 14 May 2023

Published: 17 May 2023



Copyright: © 2023 by the authors. Licensee MDPI, Basel, Switzerland. This article is an open access article distributed under the terms and conditions of the Creative Commons Attribution (CC BY) license (<https://creativecommons.org/licenses/by/4.0/>).

1. Introduction

Sources of THz radiation are widely used nowadays in science and technology [1–3]. Different applications in spectroscopy and material science [1,4–6] make its necessary to control not only the THz pulse energy but also its frequency, bandwidth and polarization state. Among the last possible applications of particular interest are (quasi)unipolar pulses that are characterized by a non-zero electric pulse area [7–10] and cause unidirectional action on charged particles [11,12].

In this paper, we develop the method proposed earlier [13,14] to control the spectral and polarization features of a THz pulse propagating in the nonequilibrium nitrogen (air) plasma channel in magnetized plasma produced by a femtosecond UV laser pulse. The main idea is based on the possibility of amplification of the THz signal in the plasma with strongly nonequilibrium electron velocity distribution function (EVDF), with the peak-like structure of this peak located in the region where the electron transport cross section increases with the energy [15,16]. Similar to [13,14], due to the cyclotron resonance, the plasma channel acts as an amplifier of the THz radiation for the angular frequencies ω close to the cyclotron frequency $\Omega_B = eB_0/mc$ (here B_0 is the induction of the external magnetic field that is directed along the plasma channel axis). Hence, through varying the induction of the external magnetic field and the plasma channel length, it is possible to change both the polarization state of the pulse and its spectral composition. Nitrogen (or air) plasma is characterized by a greater value of possible THz field amplification but at the same time by faster relaxation of the initially highly nonequilibrium EVDF in comparison with rare gases [16]. As a result, replacing the rare gas (xenon) with nitrogen (or air) as an active medium makes it possible to effectively control the spectral width of the

THz pulses in an even wider range as well as to produce rather exotic polarization states of THz pulses that cannot be described in terms of linear/elliptic/circular polarization.

Up to now, there has been a variety of possible methods for (quasi)unipolar or subcycle pulse production in different frequency ranges [17–24]. More easily, they can be in the THz range [17,18]. For example, subcycle THz pulses with given waveshapes can be generated via coherent excitation of nonlinear low-frequency oscillators through extremely short optical pulses [19]. In [20], it was proposed to form approximately unipolar half-cycle pulses via reflection of a single-cycle optical pulse from a nanometer-scale thin flat metallic or dielectric layer. In [21,22], they showed that simultaneous processes of optical rectification and multiphoton absorption of an ultrashort laser pulse in an electro-optic crystal can produce an electromagnetic precursor with a DC field component propagating ahead of the laser pulse with nearly the same field strength as in the main THz pulse. In [23], it was demonstrated that unipolar electromagnetic pulses can be generated during the interaction of an intense broadband pulse with a reflecting nonlinear medium. It was found that the static components of such unipolar pulses are equally intense during both transmission and reflection. It should be noted that all the approaches consider the case of linearly polarized quasiunipolar pulses and, in most cases, are based on one-dimensional models.

In this paper, we apply the 3D model of THz pulse propagation in the nonequilibrium magnetized plasma proposed earlier in [14] for the case of magnetized plasma in air. The model is based on the self-consistent solution of the second-order wave equation for THz electric field strength in cylindrical geometry together with the set of kinetic Boltzmann equations in the two-term expansion for the EVDF evolution in different spatial points of the channel. We analyze the data on the evolution of spectral and spatial characteristics of a THz pulse during its propagation in the channel in dependence on detuning of the central pulse frequency from the cyclotron one and for different seed pulse peak intensities. The simulations demonstrate the efficient amplification of the seed THz pulse near the resonant condition $\omega \approx \Omega_B$. We show that through applying an external magnetic field, it is possible to change the polarization state of the pulses from linear to nearly circular. In particular, the generation of (quasi)unipolar pulses with non-zero electric field areas and unusual polarization states is found to exist. Backward influence of the amplified field and fast relaxation of the EVDF in the nitrogen (air) plasma provides the possibility to produce THz pulses with significantly different central frequencies but nearly the same peak intensity and high degree of unipolarity.

2. Modeling

In this paper, we follow our model developed in [14,25]. According to this model, the femtosecond UV laser pulse (the third harmonic of Ti-Sa laser, $\hbar\Omega \approx 4.65$ eV) propagates in air at atmospheric pressure and forms the plasma channel via the three-photon ionization of O_2 molecule with a peak-like EVDF structure. For moderate laser intensities ($\sim 10^{12}$ W/cm²) four-photon ionization of N_2 molecules in accordance with perturbation theory will be significantly lower. In such case the photoelectron peak will appear at energy $\varepsilon_0 = 3\hbar\Omega - I_i \approx 1.87$ eV ($I_i \approx 12.08$ eV is the ionization potential of oxygen molecules), which approximately coincides with the middle of the energy interval ~ 1.7 – 2.2 eV corresponding to the increasing with energy of N_2 molecules transport cross section. We also note that in the energy range 0–5 eV electron transport cross section for N_2 molecules is significantly greater than for O_2 ones [26,27].

Plasma formed by a UV pulse and with a peak-like EVDF structure is the medium for amplification of low-frequency radiation (angular frequency ω is less than the electron transport frequency ν_{tr} , $\omega < \nu_{tr}$) in accordance with the mechanism proposed in [15,16]. The presence of an external magnetic field co-directional with the plasma channel axis makes it possible to amplify the radiation for larger frequencies if the inequality $|\omega - \Omega_B| < \nu_{tr}$ is satisfied. Such a situation for xenon plasma was demonstrated in [13,14].

Further, we assume that the THz pulse propagates in the nonequilibrium plasma channel formed behind the UV femtosecond pulse and located mainly in its amplifying

zone. Really, according to [16], the relaxation time of the EVDF in the nitrogen plasma is of the order of several picoseconds. Hence, the length of this zone in air is significantly shorter than in rare gases, so that even for low THz pulse intensities, this length can be smaller than the THz pulse length. In this case, the formation of a quasiunipolar pulse is possible. Here, we assume a Gaussian radial profile of electrons in the channel with homogeneous distribution over its length:

$$N_e = N_e^{(0)} \times \exp(-(\rho/R_0)^2) \tag{1}$$

Here, $N_e^{(0)}$ is on-axis electron density and R_0 is the channel radius. In analogy with [14], the electron density along the z-axis is supposed to be uniform.

The core of our model is the second-order wave equation within the cylindrical ($\vec{r} = (\rho, z)$) geometry for the electric field strength of the THz pulse $\vec{E}(\rho, z, t)$ propagating along the plasma channel (z-axis):

$$\frac{1}{\rho} \frac{\partial}{\partial \rho} \rho \frac{\partial \vec{E}(\vec{r}, t)}{\partial \rho} + \frac{\partial^2 \vec{E}(\vec{r}, t)}{\partial z^2} = \frac{1}{c^2} \frac{\partial^2 \vec{E}}{\partial t^2} + \frac{4\pi}{c^2} \frac{\partial \vec{J}(\vec{r}, t)}{\partial t} \tag{2}$$

Here, $\vec{J}(\vec{r}, t)$ is the electric current density induced by the THz pulse. To calculate this current, one should use the information on EVDF in the channel as

$$\vec{J}(\vec{r}, t) = -eN_e(\vec{r}) \int \vec{v} f(\vec{r}, \vec{v}, t) d^3v \tag{3}$$

where the EVDF is normalized according to the expression $\int f(\vec{r}, \vec{v}, t) d^3v = 1$.

In the presence of an external magnetic field, the EVDF is governed by the Boltzmann equation [28,29].

$$\frac{\partial f(\vec{r}, \vec{v}, t)}{\partial t} - \frac{e\vec{E}(\vec{r}, t)}{m} \frac{\partial f}{\partial \vec{v}} - \frac{e\vec{v} \times \vec{B}_0(\vec{r}, t)}{mc} \frac{\partial f}{\partial \vec{v}} = St(f) \tag{4}$$

Here, $St(f)$ is the collisional integral. Similar to [14], we use two-term expansion to analyze the EVDF [28]:

$$f(\vec{r}, \vec{v}, t) = f_0(\vec{r}, v, t) + \frac{\vec{v}}{v} \vec{f}_1(\vec{r}, v, t) \tag{5}$$

The symmetric part of the EVDF $f_0(\vec{r}, v, t)$ stands for the electron distribution over the absolute value of velocity, while its asymmetric part $\vec{f}_1(\vec{r}, v, t)$ determines the current response (3):

$$\vec{J}(\vec{r}, t) = -\frac{4\pi e N_e(\vec{r})}{3m} \int v^3 \vec{f}_1(\vec{r}, v, t) d^3v \tag{6}$$

Functions $f_0(\vec{r}, v, t)$ and $\vec{f}_1(\vec{r}, v, t)$ satisfy the set of equations:

$$\frac{\partial f_0(\vec{r}, v, t)}{\partial t} = \frac{e\vec{E}(\vec{r}, t)}{3mv^2} \frac{\partial}{\partial v} \left(v^2 \vec{f}_1(\vec{r}, v, t) \right) + \frac{m}{M} \frac{1}{v^2} \frac{\partial}{\partial v} \left(v_{tr}(v) \left(v f_0 + \frac{T_g}{m} \frac{\partial f_0}{\partial v} \right) \right) + Q^*(f_0) \tag{7}$$

$$\frac{\partial \vec{f}_1(\vec{r}, v, t)}{\partial t} + v_{tr}(v) \vec{f}_1 = \frac{e\vec{E}(\vec{r}, t)}{m} \frac{\partial f_0(\vec{r}, v, t)}{\partial v} + \frac{e}{mc} \vec{B}_0 \times \vec{f}_1 \tag{8}$$

Here, $v_{tr} = N\sigma_{tr}(v)v$ and $\sigma_{tr}(v)$ are the transport frequency and the transport cross section in dependence on the absolute value of velocity. $N = 2.5 \times 10^{19} \text{ cm}^{-3}$ is the gas density; M is the mass of a nitrogen molecule and $T_g = 0.025 \text{ eV}$ is the gas temperature. The collisional integral Q^* was taken in a form similar to [30]. Eight lowest vibrational

excitation cross sections were considered. Regarding the electronic excitation of nitrogen molecules, all the thresholds are above 6 eV and, hence, do not contribute to the evolution of the EVDF. The transport cross section as well as the cross sections for the vibrational excitation were taken from [26].

The initial conditions were similar to those used in [14]: The seed THz pulse is linearly polarized along the x-axis and characterized by a Gaussian profile over both z and ρ coordinates.

$$\begin{aligned} E_x(z, \rho, 0) &= E_0 \times \exp(-(\rho/\rho_0)^2) \times \\ &\exp\left(-\frac{1}{2}\left(\frac{z-z_0}{z_p}\right)^2\right) \times \left(\cos\left(\frac{\omega_0 z}{c}\right) - \sin\left(\frac{\omega_0 z}{c}\right) \times \left(\frac{z-z_0}{z_p}\right)\right), \\ E_y(z, \rho, 0) &= 0 \end{aligned} \tag{9}$$

Here, E_0 is the amplitude of the electric field, ω_0 is the carrier angular frequency, ρ_0 is the pulse transverse radius, z_p is the half-pulse duration in the spatial domain and z_0 is the position of the pulse “center of mass” relative to the leading UV pulse which is located in the point $z = 0$. Below, in our simulations, we characterize the seed pulse not via the electric field strength E_0 but via the peak intensity value, which is determined via the relation $I_0 = cE_0^2/8\pi$. It is important to note that the given expression provides a zero value of the pulse square, i.e., $\int E_x(\rho, z)\rho d\rho dz = 0$.

In analogy with [14], Equation (2) was solved numerically on the grid moving with the leading UV pulse. Hence, the UV pulse position is $z - ct = 0$ at any instant of time. Below, we assume $\rho_0 = R_0 = 1.5$ cm, $\omega_0 = 2 \times 10^{12}$ s⁻¹ and the parameter z_p is chosen as $z_p = 0.02356$ cm, which corresponds to the seed pulse half-duration $\tau_p = z_p/c \approx 7.855 \times 10^{-13}$ s. The pulse initial position is $z_0 = -5z_p \approx -0.117$ cm.

We would like to note that a rather powerful UV laser pulse with intensity $\sim 10^{12}$ W/cm² is necessary for the experimental verification of our model. Such laser pulses are available at LPI RAS [31]. However, the required pulse energy significantly exceeds the threshold for laser beams self-focusing in air (or nitrogen) that should lead to the multiple filamentation regime [32]. As a result, the radial distribution of the electrons in the channel can be significantly disturbed. It is known that the length of filament formation, or the self-focusing length [32], in such a regime is approximated using the expression [33]

$$z_f \approx \frac{0.366k\rho_0^2}{\sqrt{P/P_{cr}}} \tag{10}$$

where k is the wave vector of the laser beam, P is the beam power and P_{cr} is the power threshold of self-focusing. In our conditions, $P_{cr} \sim 100$ MW [34], while $P \sim 1$ TW. The estimation of filamentation length for the considered pulse parameters provides a value of about 100 cm, which exceeds the channel length in our study. This estimation is in agreement with recent experiment [34], where it was found that for similar pulse parameters, filaments arise at propagation length above 75 cm. Hence, here we can neglect the disturbance of the electron radial profile for propagation lengths of 30 cm.

The initial zero-order EVDF harmonic f_0 formed using a UV pulse is supposed to be characterized by the Gaussian form [30,35]:

$$f_0(\rho, z = ct, v) = \frac{1}{4\pi} \frac{m^{\frac{3}{2}}}{\Delta\varepsilon \sqrt{2\pi(mv^2/2)}} \times \exp\left(-\frac{(mv^2/2 - \varepsilon_0)^2}{\Delta\varepsilon^2}\right) \tag{11}$$

with $\varepsilon_0 = 1.87$ eV and $\Delta\varepsilon = 0.1$ eV. With regard to the asymmetric part f_1 , we neglect the anisotropy of the photoionization process, hence:

$$f_1(\rho, z = ct, v) \equiv 0 \tag{12}$$

The wave Equation (2) for x- and y-components of the electric field vector is solved jointly with the set of Equations (7) and (8) at each spatial grid point. Similar to [36],

the temporal step of integration is $\Delta t = 4 \times 10^{-15}$ s, the step of space discretization is $\Delta z = c \times \Delta t = 1.2 \times 10^{-4}$ cm and $\Delta \rho = 0.065$ cm. The total spatial area for calculations is chosen as $\ell = 1.0$ cm and $R_{max} = 6.0$ cm.

3. Results and Discussion

3.1. Control of the Carrier Pulse Frequency State in the Magnetized Nonequilibrium Plasma Channel

We start the analysis of initially linearly polarized THz pulse propagation in air with a magnetized plasma channel in air for different seed pulse intensities in dependence on the value of the induction of a static magnetic field directed along the plasma channel. The initial spatial structure of the THz pulse and its spectral composition are shown in Figure 1. We note that the pulse is approximately single-cycle and characterized by a wide spectral band. This fact allows us to tune the central frequency in a wide range. We consider the range of magnetic field induction $B_0 = 0 \div 4 \times 10^5$ G that corresponds to cyclotron frequencies $\Omega_B = 0 \div 7 \times 10^{12}$ s⁻¹.

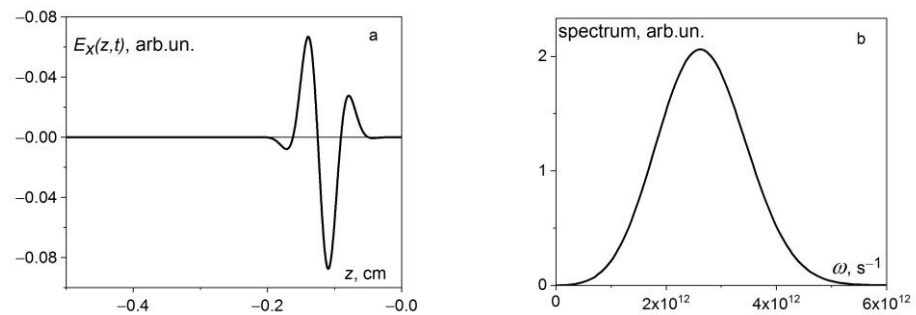


Figure 1. Initial ($t = 0$) THz pulse: spatial distribution of electric field strength (a) and its spectral composition (b).

Both initial pulse structure and structure after the 30 cm length propagation for different values of cyclotron frequency are shown in Figure 2. In all the cases under study, one can see that a transformation from linear polarization to nearly circular polarization (the absolute value of electric field does not oscillate in time) is observed during the propagation. This transformation is accompanied by significant pulse amplification. We also note that the nearly circular polarization is formed at a propagation length of approximately 6 cm (see Figure 3).

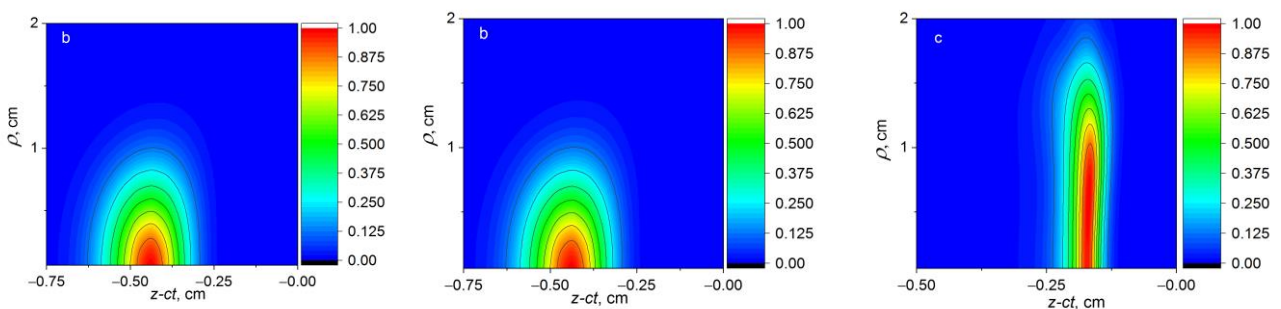


Figure 2. 3D spatial distribution of the absolute value of the electric field strength in the THz pulse: initial distribution (a), after 30 cm length propagation in the magnetized nonequilibrium air plasma channel with Gaussian profile of electron density with $N_e^{(0)} = 7 \times 10^{13}$ cm⁻³; $\Omega_B = \omega_0 = 2 \times 10^{12}$ s⁻¹: (b) $I_0 = 1$ W/cm² and (c) $I_0 = 10^5$ W/cm². Radial sizes of channel and seed THz pulse are $R_0 = \rho_0 = 1.5$ cm. The level lines are normalized to the electric field maximum value. The femtosecond UV pulse is located at the point $z - ct = 0$. For case (c), THz pulse compression results from the essential EVDF reconstruction.

To analyze the amplification properties of the air plasma channel in the presence of an external magnetic field, we introduce the gain factor G , representing the ratio of the pulse energy at the propagation distance L to the initial pulse energy

$$g(L) = \int E^2(\rho, z, t = L/c) \rho d\rho dz / \int E^2(\rho, z, t = 0) \rho d\rho dz \quad (13)$$

where the integrals are taken over the entire spatial area including $\rho > \rho_0$.

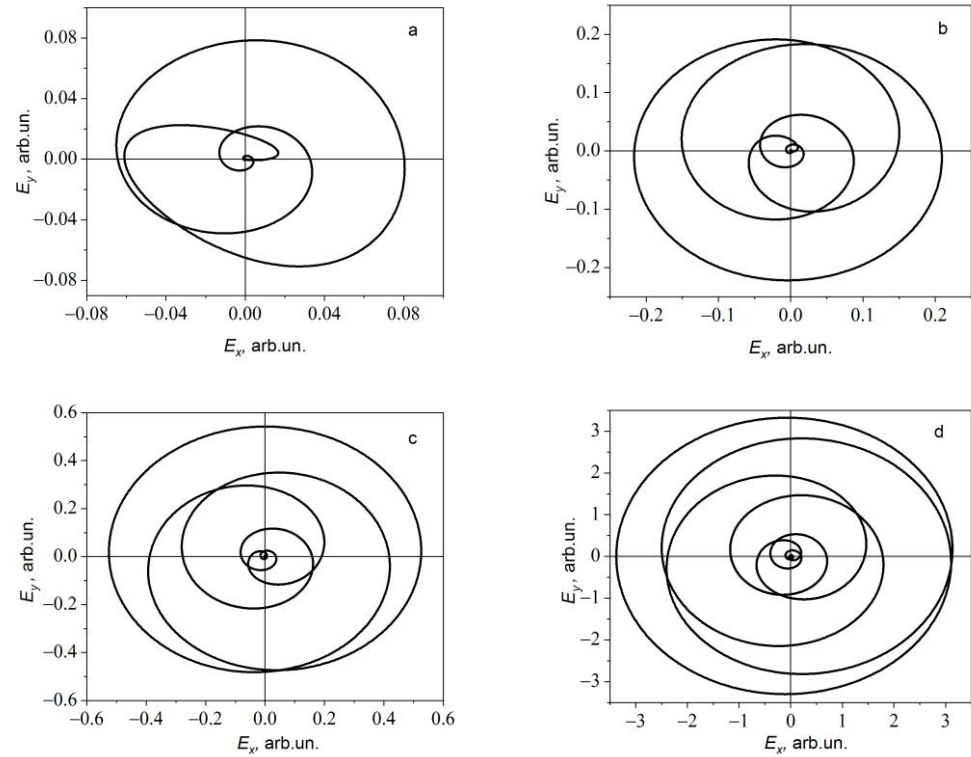


Figure 3. Polarization state of the amplified THz pulse, $E_y(E_x)$ for different propagation lengths in the channel: (a) 3 cm, (b) 6 cm, (c) 9 cm, (d) 15 cm. The cyclotron frequency is $\Omega_B = 2 \times 10^{12} \text{ s}^{-1}$. The electric field vector rotates counterclockwise.

The obtained data for THz gain depending on the cyclotron frequency Ω_B for two values of seed pulse peak intensity are presented in Figure 4. First, for low initial pulse intensity, one can see dramatic enhancement (more than two orders of magnitude) of the gain in a rather narrow range near the cyclotron frequency (curve 1). On the other hand, we observe a nearly flat dependence (curve 2) of the gain at a level of $G = 30 - 100$ for the cyclotron frequency from zero value up to $5 \times 10^{12} \text{ s}^{-1}$. That is the consequence of the backward influence of the amplified THz pulse on the EVDF that results in fast degradation of the photoionization peak during the pulse propagation and amplification (see Figure 5). Data in Figure 5a correspond to the weak seed pulse amplification when the THz pulse does not perturb the EVDF evolution. On the contrary, the initial intensity in Figure 5b is 10^4 W/cm^2 , which causes the essential broadening of the EVDF peak. As a result, there is a decrease in the gain and saturation of the maximum value of the output signal. To demonstrate this saturation effect, we calculate the dependence of the output THz pulse energy on the initial seed pulse intensity for the 30 cm plasma channel and two values of cyclotron frequency: the resonant one— $\Omega_B = 2 \times 10^{12} \text{ s}^{-1}$ and nonresonant one— $\Omega_B = 5 \times 10^{11} \text{ s}^{-1}$ (see Figure 6). We calculate the output THz pulse energy as

$$Q(L) = \frac{c}{4} \int E^2(\rho, z, t = L/c) \rho d\rho dz \quad (14)$$

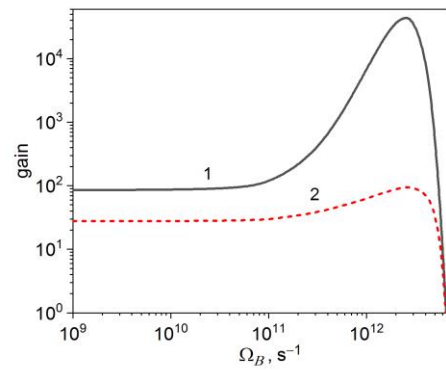


Figure 4. Gain for the propagation distance $L = 30$ cm depending on the cyclotron frequency for initial peak intensities 1 W/cm^2 (curve 1) and 10^4 W/cm^2 (curve 2).

We see that the gain is much greater for the resonant case, but for both cyclotron frequencies, the curves are saturated at the level of $\sim 10^{-5} \text{ J}$, which corresponds to the peak pulse intensities close to 10^6 W/cm^2 .

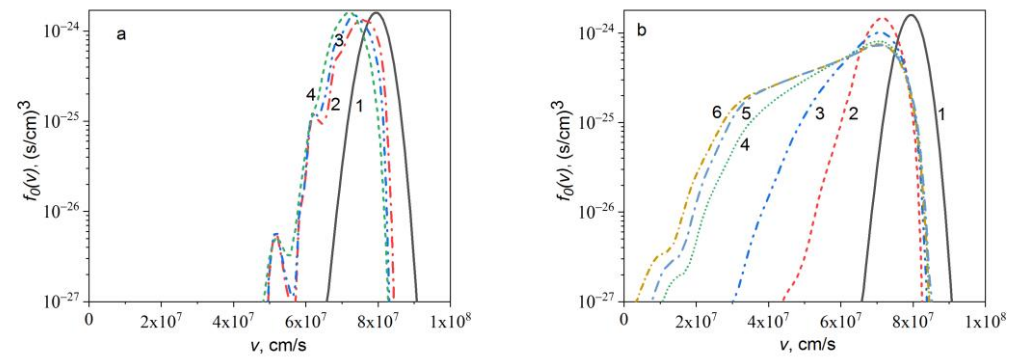


Figure 5. (a) On-axis electron velocity distribution functions for the propagation length 30 cm in the spatial points behind the UV pulse: initial EVDF (1); $z - ct = -0.1 \text{ cm}$ (2) -0.2 cm (3) and -0.4 cm (4) for $I_0 = 0.1 \text{ W/cm}^2$. (b) On-axis electron velocity distribution functions for the spatial point $z - ct = -0.4 \text{ cm}$ and different propagation lengths: 0 (1), 3 cm (2), 6 cm (3), 9 cm (4), 15 cm (5), 30 cm (6) for $I_0 = 10^4 \text{ W/cm}^2$.

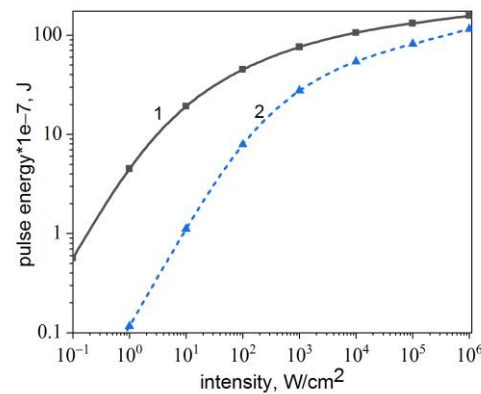


Figure 6. The dependence of THz pulse energy on the initial seed pulse intensity for the 30 cm propagation length: the cyclotron frequency is (1) $\Omega_B = 2 \times 10^{12} \text{ s}^{-1}$, (2) $\Omega_B = 5 \times 10^{11} \text{ s}^{-1}$.

To provide more insight into the effect of resonance amplification of the THz pulse in the channel, we demonstrate on-axis spectra of the pulses (see Figure 7) after 30 cm propagation in the plasma channel for different values of the cyclotron frequency and two

initial intensities, $I_0 = 0.1 \text{ W/cm}^2$ (a) and 10^4 W/cm^2 (b). These spectra are calculated as $I_\omega \sim \omega^4(|E_\omega^{(x)}|^2 + |E_\omega^{(y)}|^2)$, where $E_\omega^{(x)}$ and $E_\omega^{(y)}$ are the Fourier decomposition of the x- and y-components of the electric field vector. For the low intensity limit ($I_0 = 0.1 \text{ W/cm}^2$), the amplification width is in the range $1 \div 4 \times 10^{12} \text{ s}^{-1}$ and corresponds approximately to the bandwidth of the seed pulse. If the seed pulse intensity increases, the amplification bandwidth also increases: for the initial intensity $I_0 = 10^4 \text{ W/cm}^2$, effective amplification is possible within the frequency range of $0.3 \div 6 \times 10^{12} \text{ s}^{-1}$ with nearly the same gain. This means that the magnetized plasma channel can be used for effective tuning of the THz pulse carrier frequency.

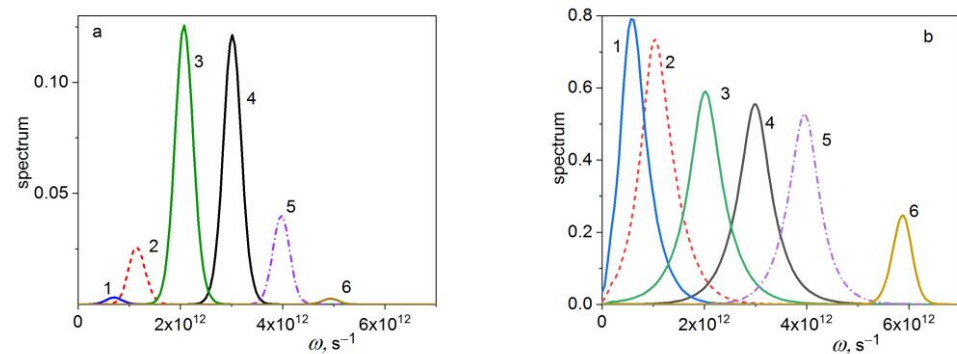


Figure 7. On-axis spectra of THz pulse after the 30 cm propagation in channel for seed pulse intensity $I_0 = 0.1 \text{ W/cm}^2$ (a) and 10^4 W/cm^2 (b) and different values of cyclotron frequency (in s^{-1}): (1) 5×10^{11} ; (2) 10^{12} ; (3) 2×10^{12} ; (4) 3×10^{12} ; (5) 4×10^{12} ; (6) 5×10^{12} for (a) and 6×10^{12} for (b).

3.2. Unipolar Pulse Generation with Unique Polarization Features

In this chapter, we analyze the features of so-called quasiunipolar pulses that can be generated from a magnetized plasma channel. Unipolar pulses or pulses with non-zero electric pulse area were first proposed in [37], where the pulse area was introduced as the time-integrated electric field strength at any spatial point:

$$S(\vec{r}) = \int E(\vec{r}, t) dt \tag{15}$$

For the (quasi)unipolar pulses, integral (15) has a non-zero value. Such definition of pulse area is widely used in a number of recent papers [8,11,12,18–23,38–41]. On the other hand, the pulse area can be introduced in another way, as the integral over the spatial coordinates [14]

$$S(t) = \int E(\vec{r}, t) d^3r. \tag{16}$$

Evidently, these definitions are not equivalent to each other. The only exception is the one-dimensional propagation of an electromagnetic wave in the nondispersive medium. Really, every function $E(z, t) = E(z \mp ct)$ (c is the speed of light in vacuum in nondispersive medium) of the retarded/leading argument $\zeta = z \mp ct$ is the solution of the second-order wave equation

$$\frac{\partial^2 E(z, t)}{\partial z^2} = \frac{1}{c^2} \frac{\partial^2 E(z, t)}{\partial t^2}. \tag{17}$$

It means that for the case under study, the integrals (15) and (16) are bound by the relation

$$\int E(z, t) dz = c \int E(z, t) dt \tag{18}$$

and do not depend on time and spatial coordinate and can have non-zero value even in free space.

The case of propagation in 3D geometry is much more complicated. Pulses with a zero-frequency component can arise in different media, both solid and gaseous, while in the free

space, they cannot have a zero-frequency component [18]. In [25], it was demonstrated that the degree of pulse unipolarity rapidly drops after transferring the pulse with non-zero area into the free space from the plasma channel. It can be argued that in such a situation, much of the theoretical research that analyzed the formation and propagation of one-dimensional unipolar pulses should be verified for 3D geometry.

Below, we will use the pulse area defined using expression (16). We should stress that if the pulse is not linearly polarized and changes its polarization state during the propagation, one needs the vector generalization of expression (16):

$$\vec{S}(t) = \begin{Bmatrix} S_x \\ S_y \end{Bmatrix} = 2\pi \int \begin{Bmatrix} E_x(\rho, z, t) \\ E_y(\rho, z, t) \end{Bmatrix} \rho d\rho dz \tag{19}$$

Further, we define the unipolar factor as follows:

$$U(t) = \frac{1}{2\pi} \left(\frac{|S_x|}{\int |E_x(\rho, z, t)| \rho d\rho dz} + \frac{|S_y|}{\int |E_y(\rho, z, t)| \rho d\rho dz} \right) \tag{20}$$

The value obtained from (20) can vary in the range $U = 0 - 2$. For the case of linear polarized pulse, expression (20) coincides with those used in [14].

The mechanism of quasiunipolar pulses formation during THz pulse propagation in a nitrogen (air) plasma channel is as follows. Fast relaxation of the EVDF results in the dominant amplification of the leading front of the pulse compared to its trailing edge [25]. The effect of spatially inhomogeneous pulse amplification becomes more pronounced for rather intense seed THz pulses when the backward influence of the amplified field on the EVDF additionally contributes to its reconstruction. The presence of an external magnetic field can additionally advance the effect of unipolarity formation. Indeed, if one chooses a cyclotron frequency below the carrier frequency, the spectral components of the amplified pulse will be shifted down (see data in Figure 7). It means that for the same pulse duration, the number of field oscillations decreases down to unity and less. In such situations, even weak spatial inhomogeneity of the amplification can lead to the formation of pulse unipolarity.

The data on the unipolar factor U for different cyclotron frequencies in dependence on the peak intensity of the seed THz pulse (see Figure 8) confirm the aforementioned analysis. One can see that the unipolar factor increases with seed THz pulse intensity increment. This increment is much more pronounced for the cyclotron frequency below the carrier frequency (see Figure 8a). The dependence of the U -factor on cyclotron frequency for the concrete value of initial pulse intensity ($I_0 = 10^4 \text{ W/cm}^2$, carrier frequency $\omega_0 = 2 \times 10^{12} \text{ s}^{-1}$) is plotted in Figure 8b. We obtain that the unipolar factor increases from a near-zero value at $\Omega_B = 3 \times 10^{12} \text{ s}^{-1}$ to approximately $U \approx 1.2$ for $\Omega_B \leq 10^{11} \text{ s}^{-1}$.

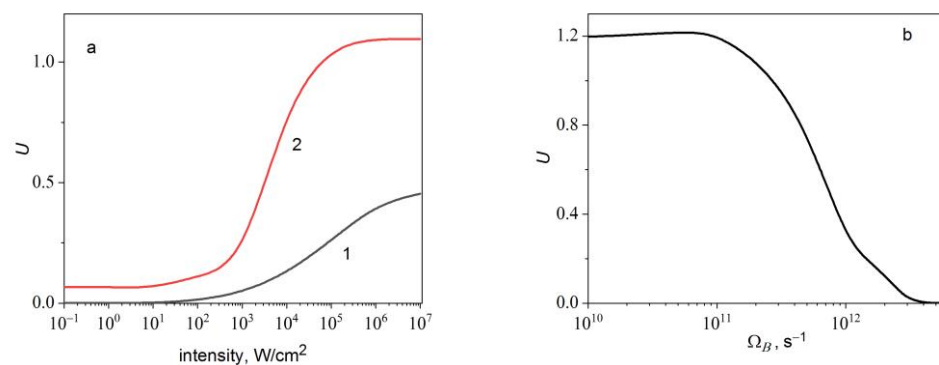


Figure 8. (a) Unipolar factor in dependence on the seed pulse peak intensity for cyclotron frequencies $\Omega_B = 2 \times 10^{12} \text{ s}^{-1}$ (1) and $\Omega_B = 5 \times 10^{12} \text{ s}^{-1}$ (2); (b) unipolar factor in dependence on the cyclotron frequency for the seed pulse intensity $I_0 = 10^4 \text{ W/cm}^2$.

We should mention that the polarization properties of the quasiunipolar pulses produced in the magnetized plasma can be rather specific. Really, the polarization states of a quasiunipolar pulse formed in a magnetized plasma channel for different relations between cyclotron and carrier frequencies Ω_B/ω_0 and different seed pulse intensities are plotted in Figure 9. The degree of unipolarity increases with the growth of seed pulse intensity and the decrement of the ratio Ω_B/ω_0 . It is also important that the polarization state of such pulses cannot be characterized using conventional definitions such as linear, circular or elliptic polarization. The electric field vector draws a rather complicated curve in the space that demonstrates the electric force action dominantly in certain directions, which provides a kick for both translational and rotational motion of electrons in molecules. We suppose that such pulses will be of special interest for spectroscopy of macromolecules and chiral structures. Unusual polarization properties of extremely short pulses were also discussed in a recent review [42], where the production of THz pulses via optical pumping in a Bi_2Te_3 crystal was considered.

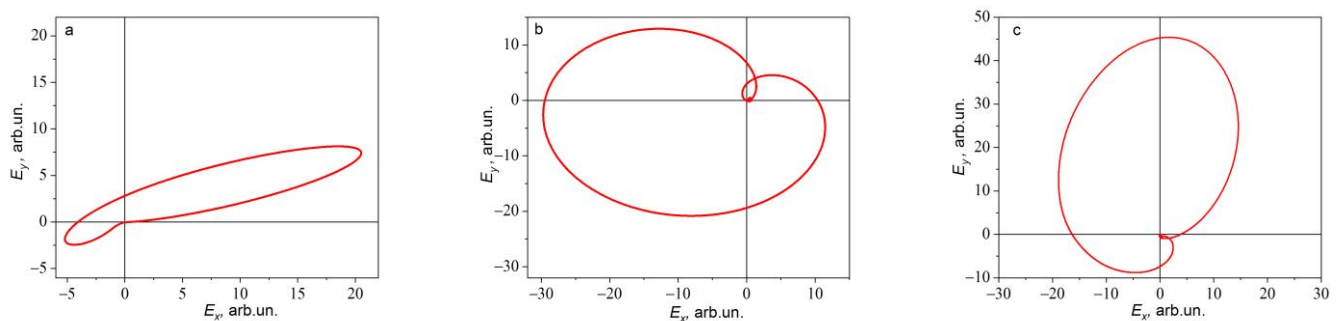


Figure 9. Polarization state of the unipolar THz pulse, $E_y(E_x)$, after the 30 cm propagation length in the channel: $\Omega_B = 5 \times 10^{10} \text{ s}^{-1}$, $I_0 = 10^4 \text{ W/cm}^2$ (a), $\Omega_B = 5 \times 10^{11} \text{ s}^{-1}$, $I_0 = 10^4 \text{ W/cm}^2$ (b), $\Omega_B = 5 \times 10^{11} \text{ s}^{-1}$, $I_0 = 10^6 \text{ W/cm}^2$. (c) The carrier seed pulse frequency $\omega = 2 \times 10^{12} \text{ s}^{-1}$. The electric field vector rotates counterclockwise.

4. Conclusions

In summary, we have developed a self-consistent three-dimensional model to analyze terahertz pulse propagation and amplification in a nonequilibrium air (nitrogen) magnetized plasma channel formed via multiphoton ionization using a femtosecond UV laser pulse. The ability to tune the central frequency of the THz pulse in a wide range of parameters is demonstrated. The results reveal the possibility of generating (quasi)unipolar pulses with unusual polarization states through applying an external magnetic field. This research is highly relevant and significant in the field of THz science as well as in quantum mechanics, as it offers new approaches for analyzing kick-type action on quantum systems for both translational and rotational motion.

Author Contributions: Conceptualization, A.V.B.; data curation, A.M.P.; investigation, A.V.B.; software, E.A.V.; supervision, A.V.B. and A.M.P.; writing—original draft, A.M.P.; Writing—review and editing, A.V.B. All authors have read and agreed to the published version of the manuscript.

Funding: Authors (A.V.B. and A.M.P.) thank the Russian Science Foundation, Grant No. 22-22-00225.

Institutional Review Board Statement: Not applicable.

Informed Consent Statement: Not applicable.

Data Availability Statement: Data underlying the results presented in this paper are not publicly available at this time but may be obtained from the authors upon reasonable request.

Acknowledgments: We thank R. Arkhipov and N. Rosanov for the discussion of the physics of unipolar pulses.

Conflicts of Interest: The authors declare no conflict of interest.

References

1. Tonouchi, M. Cutting-edge terahertz technology. *Nat. Photonics* **2007**, *1*, 105. [[CrossRef](#)]
2. Kampfrath, T.; Tanaka, K.; Nelson, K. Resonant and nonresonant control over matter and light by intense terahertz transients. *Nat. Photonics* **2013**, *7*, 680. [[CrossRef](#)]
3. Jepsen, P.; Cooke, D.; Koch, M. Terahertz spectroscopy and imaging—Modern techniques and applications. *Laser Photonics Rev.* **2011**, *5*, 124–166. [[CrossRef](#)]
4. Yang, X.; Zhao, X.; Yang, K.; Liu, Y.; Liu, Y.; Fu, W.; Luo, Y. Biomedical Applications of Terahertz Spectroscopy and Imaging. *Trends Biotechnol.* **2016**, *34*, 810–824. [[CrossRef](#)] [[PubMed](#)]
5. Hoshina, H.; Morisawa, Y.; Sato, H.; Minamide, H.; Noda, I.; Ozaki, Y.; Otani, C. Polarization and temperature dependent spectra of poly(3-hydroxyalkanoate)s measured at terahertz frequencies. *Phys. Chem. Chem. Phys.* **2011**, *13*, 9173. [[CrossRef](#)]
6. Katletz, S.; Pflieger, M.; Pühringer, H.; Mikulics, M.; Vieweg, N.; Peters, O.; Scherger, B.; Scheller, M.; Koch, M.; Wiesau, K. Polarization sensitive terahertz imaging: Detection of birefringence and optical axis. *Opt. Express* **2012**, *20*, 23025–23035. [[CrossRef](#)]
7. Rosanov, N. Area of ultimately short light pulses. *Opt. Spectrosc.* **2009**, *107*, 721–725. [[CrossRef](#)]
8. Arkhipov, R.; Arkhipov, M.; Pakhomov, A.; Babushkin, I.; Rosanov, N. Half-cycle and unipolar pulses (Topical Review). *Laser Phys. Lett.* **2022**, *19*, 043001. [[CrossRef](#)]
9. Chai, X.; Ropagnol, X.; Raeis-Zadeh, S.M.; Reid, M.; Safavi-Naeini, S.; Ozaki, T. Subcycle Terahertz Nonlinear Optics. *Phys. Rev. Lett.* **2018**, *121*, 143901. [[CrossRef](#)]
10. Sychugin, S.; Novokovskaya, A.; Bakunov, M. Propagation dynamics of optically generated unipolar electromagnetic pulses. *Phys. Rev. A* **2022**, *105*, 053528. [[CrossRef](#)]
11. Arkhipov, R.; Pakhomov, A.; Arkhipov, M.; Babushkin, I.; Demircan, A.; Morgner, U.; Rosanov, N. Unipolar subcycle pulse-driven nonresonant excitation of quantum systems. *Opt. Lett.* **2019**, *44*, 1202–1205. [[CrossRef](#)] [[PubMed](#)]
12. Pakhomov, A.; Arkhipov, M.; Rosanov, N.; Arkhipov, R. Ultrafast control of vibrational states of polar molecules with subcycle unipolar pulses. *Phys. Rev. A* **2022**, *105*, 043103. [[CrossRef](#)]
13. Bogatskaya, A.; Gnezdovskaia, N.; Popov, A. Circularly polarized terahertz pulses generation in plasma channel created by the UV high-intense laser pulse in the presence of static magnetic field. *Phys. Rev. E* **2020**, *102*, 043202. [[CrossRef](#)]
14. Bogatskaya, A.; Volkova, E.; Popov, A. Polarization and frequency-controlled amplification in a nonequilibrium plasma in the presence of an external magnetic field. *Plasma Sour. Sci. Technol.* **2022**, *31*, 095009.
15. Bogatskaya, A.; Popov, A. On the possibility of the amplification of subterahertz electromagnetic radiation in a plasma channel created by a high intensity ultrashort laser pulse. *JETP Lett.* **2013**, *97*, 388. [[CrossRef](#)]
16. Bogatskaya, A.; Volkova, E.; Popov, A. On the possibility of a short subterahertz pulse amplification in a plasma channel created in air by intense laser radiation. *J. Phys. D* **2014**, *47*, 185202. [[CrossRef](#)]
17. Roskos, H.G.; Tomson, M.D.; Kress, M.; Löfer, T. Broadband THz emission from gas plasmas induced by femtosecond optical pulses: From fundamentals to applications. *Laser Photonics Rev.* **2017**, *1*, 349–368. [[CrossRef](#)]
18. Reimann, K. Table-top sources of ultrashort THz pulses. *Rep. Progr. Phys.* **2007**, *70*, 1597. [[CrossRef](#)]
19. Pakhomov, A.V.; Arkhipov, R.M.; Arkhipov, M.V.; Demircan, A.; Morgner, U.; Rosanov, N.N.; Babushkin, I.V. Unusual terahertz waveforms from a resonant medium controlled by diffractive optical elements. *Sci. Rep.* **2019**, *9*, 7444. [[CrossRef](#)]
20. Arkhipov, M.V.; Arkhipov, R.M.; Pakhomov, A.V.; Babushkin, I.V.; Demircan, A.; Morgner, U.; Rosanov, N.N. Generation of unipolar half-cycle pulses via unusual reflection of a single-cycle pulse from an optically thin metallic or dielectric layer. *Opt. Lett.* **2017**, *42*, 2189–2192. [[CrossRef](#)]
21. Bakunov, M.I.; Maslov, A.V.; Tsarev, M.V. Optically generated terahertz pulses with strong quasistatic precursor. *Phys. Rev. A* **2017**, *95*, 063817. [[CrossRef](#)]
22. Tsarev, M.V.; Bakunov, M.I. Titled-pulse-front excitation of strong quasistatic precursors. *Opt. Express* **2019**, *27*, 5154. [[CrossRef](#)]
23. Kozlov, V.V.; Rosanov, N.N.; Angelis, C.D.; Wabnitz, S. Generation of unipolar pulses from nonunipolar optical pulses in a nonlinear medium. *Phys. Rev. A* **2011**, *84*, 023818. [[CrossRef](#)]
24. Shou, Y.; Hu, R.; Gong, Z.; Yu, J.; Chen J-e Mourou, G.; Yan, X.; Ma, W. Cascaded generation of isolated sub-10 attosecond half-cycle pulses. *New J. Phys.* **2021**, *23*, 053003. [[CrossRef](#)]
25. Bogatskaya, A.; Volkova, E.; Popov, A. On the possibility of intense unipolar THz pulses formation in nonhomogeneous nonequilibrium nitrogen plasma channels. *Photonics* **2023**, *10*, 113. [[CrossRef](#)]
26. Phelps, A.; Pitchford, L. Anisotropic scattering of electrons by N₂ and its effects on electron transport: Tabulations of cross section and results. In *JILA Information Center Report*; No 26; University of Colorado: Boulder, CO, USA, 1985.
27. Phelps, A.; Van Brunt, R. Electron-transport, ionization, attachment, and dissociation coefficients in SF₆ and its mixtures. *J. Appl. Phys.* **1988**, *64*, 4269. [[CrossRef](#)]
28. Ginzburg, V.; Gurevich, A. Nonlinear phenomena in a plasma located in an altering electromagnetic field. *Sov. Phys. Usp.* **1960**, *3*, 115. [[CrossRef](#)]
29. Raizer, Y. *Laser-Induced Discharge Phenomena*; Consultants Bureau: New York, NY, USA, 1977.
30. Bogatskaya, A.; Volkova, E.; Popov, A. Unipolar terahertz pulse formation in a nonequilibrium plasma channel formed by an ultrashort uv laser pulse. *Phys. Rev. E* **2021**, *104*, 025202. [[CrossRef](#)]

31. Zvorykin, V.; Goncharov, S.; Ionin, A.; Mokrousova, D.; Ryabchuk, S.; Seleznev, L.; Sunchugasheva, E.; Ustinovskii, N.; Shutov, A. Experimental capabilities of the GARPUN MTW Ti: Sapphire—KrF laser facility for investigating the interaction of subpicosecond UV pulses with targets. *Quantum Electron.* **2017**, *47*, 319. [[CrossRef](#)]
32. Chekalin, S.; Kandidov, V. From self-focusing light beams to femtosecond laser pulse filamentation. *Phys. Usp.* **2013**, *56*, 123. [[CrossRef](#)]
33. Kelley, P. Self-focusing of optical beams. *Phys. Rev. Lett.* **1965**, *15*, 1005. [[CrossRef](#)]
34. Shipilo, D.; Panov, N.; Suchungasheva, E.; Mokrousova, D.; Shutov, A.; Zvorykin, V.; Ustinovskii, N.; Seleznev, L.; Savel'ev, A.; Kosareva, O.; et al. Fifteen meter long uninterrupted filaments from sub-terawatt ultraviolet pulse in air. *Opt. Express* **2017**, *25*, 25386. [[CrossRef](#)] [[PubMed](#)]
35. Bogatskaya, A.; Volkova, E.; Popov, A. New method of unipolar THz pulse generation in photoionised xenon plasma. *Plasma Sources Sci. Technol.* **2021**, *30*, 085001. [[CrossRef](#)]
36. Bogatskaya, A.; Volkova, E. 3D modeling of short THz pulse propagation and amplification in the nonequilibrium plasma channel. *JOSA B* **2022**, *39*, 299. [[CrossRef](#)]
37. Bessonov, E. On a class of electromagnetic waves. *Sov. Phys. JETP* **1981**, *53*, 433.
38. Arkhipov, R.; Pakhomov, A.; Arkhipov, M.; Demircan, A.; Morgner, U.; Rosanov, N.; Babushkin, I. Selective ultrafast control of multi-level quantum systems by subcycle and unipolar pulses. *Opt. Express* **2020**, *28*, 17020–17034. [[CrossRef](#)]
39. Rosanov, N. On acceleration of a relativistic particle by a radiation pulse. *Opt. Spectrosc.* **2019**, *126*, 140–143. [[CrossRef](#)]
40. Rosanov, N.; Tumakov, D.; Arkhipov, M.; Arkhipov, R. Criterion for the yield of micro-object ionization driven by few- and subcycle radiation pulses with nonzero electric area. *Phys. Rev. A* **2021**, *104*, 063101. [[CrossRef](#)]
41. Arkhipov, M.; Arkhipov, R.; Rosanov, N. Obtaining Unipolar Pulses at Far Field Zone of the Source. *Opt. Spectrosc.* **2021**, *129*, 1193–1195. [[CrossRef](#)]
42. Arkhipov, R.M.; Arkhipov, M.V.; Pakhomov, A.V.; Obraztsov, P.A.; Rosanov, N.N. Unipolar and Subcycle Extremely Short Pulses: Recent Results and Prospects (Brief Review). *JETP Lett.* **2023**, *117*, 8–23. [[CrossRef](#)]

Disclaimer/Publisher's Note: The statements, opinions and data contained in all publications are solely those of the individual author(s) and contributor(s) and not of MDPI and/or the editor(s). MDPI and/or the editor(s) disclaim responsibility for any injury to people or property resulting from any ideas, methods, instructions or products referred to in the content.